NJC

Accepted Manuscript

This article can be cited before page numbers have been issued, to do this please use: S. Nath, S. K. Pathak, B. Pradhan, R. K. Gupta, K. Anki Reddy, G. Krishnamoorthy and A. Ammathnadu Sudhakar, *New J. Chem.*, 2018, DOI: 10.1039/C7NJ05136K.

ROYAL SOCIETY OF CHEMISTRY

rsc.li/njc

View Article Online
DOI: 10.1039/C7NJ05136K

A Sensitive and Selective Sensor for Picric Acid Detection with a Fluorescence Switching Response

Subrata Nath,[a] Suraj Kumar Pathak, [a] Balaram Pradhan, [a] Ravindra Kumar Gupta,[a] K. Anki Reddy,[b] G. Krishnamoorthy,[a*] and A. S. Achalkumar [a*]
[a]Department of Chemistry, [b]Department of Chemical Engineering, Indian Institute of Technology Guwahati, Guwahati-781039, Assam, India.

ABSTRACT: A low molecular weight organogelator containing 3,5-substituted-1,3,4-oxadiazole and tetrazole units was synthesized and characterized. This compound was only soluble in DMSO and forms a stable gel. The solution and gel exhibit a blue light emission. The gel was characterized by atomic force microscopy, field-emission scanning electron microscopy, ^{1}H NMR and fluorescence measurements. The gel to solution interconversion was reversible for many cycles of heating and cooling. The compound in solution exhibited a high selectivity for the detection of common explosive and water pollutant picric acid. Fluorimetric titration studies with nitro explosive compounds revealed that emission of the compound was red shifted in response to the addition of picric acid, and exhibited a shifting of fluorescence from blue to green. Theoretical and experimental studies revealed that the sensing is due to the complexation of picrate anion with the protonated fluorophore. The shifting of emission in response to picric acid in the visual region is ideal for the naked eye detection of the explosives and therefore it is promising in comparison to the detection methods based on fluorescence quenching.

INTRODUCTION

Sensitive and selective detection of explosives is an area of paramount importance in the present era. The increasing number of terror attacks on human civilization is pressing scientists to device an effective way to detect explosives. Apart from this, increasing industrial effluents are causing severe damages to our environment by contaminating the land and water bodies, posing serious health related hazards. Picric acid (PA) is a very powerful explosive, which is even stronger than trinitrotoluene (TNT).[1] Phenols are one of the most common organic water pollutants due to the high solubility and toxicity at very low concentrations. Out of various phenol derivatives, picric acid or 2,4,6-trinitro phenol is a strong organic acid and highly toxic.[1] It seriously affects human eyes, skin and respiratory systems, liver malfunction, and also causes chronic diseases like anemia, cancer, and cyanosis.[2] In spite of that, it's use is inevitable in dye industries, pharmaceuticals, rocket fuel manufacturing, and chemical laboratories.[3] As a result of it's widespread use in several industries and high water solubility, it is contaminating water and

View Article Online
DOI: 10.1039/C7NJ05136K

soil. The specific recognition of PA remains a challenging task for researchers because of the similar electron deficient nature of all the nitro explosives and other phenolic contaminants. Various methodologies based on spectroscopic,[4] electrochemical techniques have been utilized for this purpose. [5] Similarly, several small molecule sensors,[6] nanoparticles,[7] nanofibers,[8] gels [9] polymers[10] and metal organic frameworks (MOFs)[11] etc. have been designed for the detection of picric acid. Among these different techniques, especially the fluorescence sensors have high potential and advantages, because of their high sensitivity, cost efficiency, portability, simple instrumentation, easy sample preparation and quick response. This field has caught the attention of researchers and hence several fluorescent sensors for PA have been reported, even though a decade has passed after the first report on a selective PA sensor.[12] Notably, many of these fluorescent sensors show fluorescence quenching in response to PA, but the sensors which show a shift in the emission in response to PA are rare.[13] Shifting of emission in the visible region produce a change in the emission color, which eases the detection process, thus enabling the naked eye detection with the minimization of errors in the detection. Further, it is challenging to develop such a sensor, which detects the PA with high selectivity and low detection limit.

Gelators are a class of self-assembled soft matter, which are finding increasing applications in tissue engineering, drug delivery, sensors, light harvesting and photo responsive systems.[14] Tetrazoles form an important class of 5-membered heterocyclic compounds, with a high range of pharmacological and biological activity. The acidic proton of 1-H-tetrazole can form hydrogen bonding (H-bonding) with any electronegative atoms and its application as a fluoride sensor has been reported recently due to its low pKa (3-5) value.[15] In the present work, we report a low molecular weight gelator **1** that consists of a tetrazole unit, a substituted 1,3,4-oxadiazole unit, and long flexible alkyl chains (Fig.1). The oxadiazole unit serves as a fluorophore, the long alkyl chains were selected for their hydrophobic interaction and for stabilizing gelation, while the tetrazole unit acts as a polar unit with an ability to form H-bonding. Tetrazole moiety has been utilized in the molecular design of calamitic[16a-c] and metal containing mesogens.[16d] This has been also utilized in the stabilization of hydrogels[17a-b] and organogels.[17c-d] However, reports on tetrazole containing gelators, especially used for the sensing purpose of aromatic explosives in the gel state remain rare.[17e-f]

View Article Online
DOI: 10.1039/C7NJ05136K

RESULTS AND DISCUSSION

Synthesis and characterization

The detailed synthetic route is provided in scheme 1. Ethyl-3,4,5-trihexadecyloxybenzoate (**5**) was obtained from ethyl-3,4,5-trihydroxybenzoate by *O*-alkylation, following the Willimson's

Scheme 1

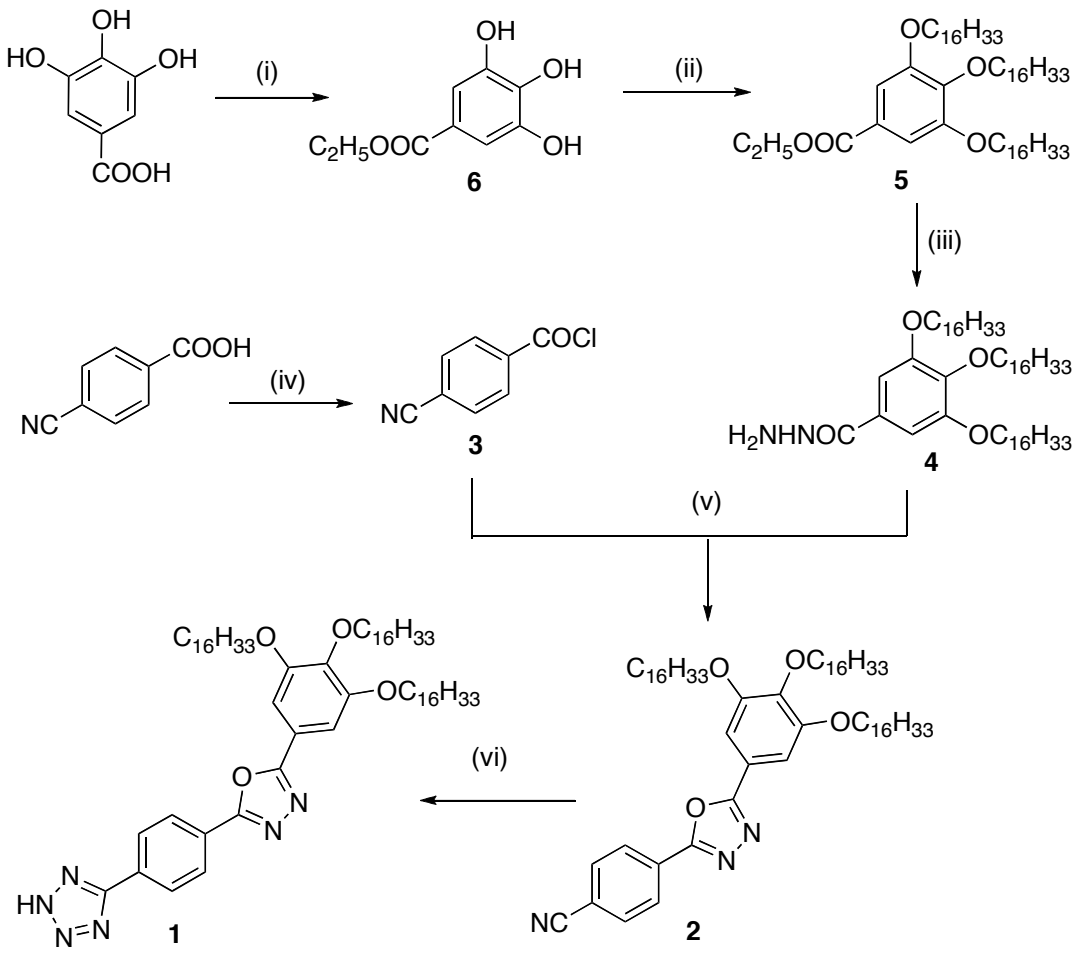

Reagents and conditions: (i) Ethanol, H_2SO_4, reflux, 24 h, 70%; (ii) $C_{16}H_{33}Br$, DMF, 80 ^oC, 24 h, 75%; (iii) Ethanol, $N_2H_4.H_2O$, reflux, 48 h, 67% (iv) $SOCl_2$, DMF, reflux, 4 h; (v) (a) THF, TEA, reflux, 12 h; (b) $POCl_3$, reflux, 12 h, 70%; (vi) NaN_3, NH_4Cl, DMF, 120 ^oC, 48 h, 56%.

ether synthesis protocol. This ester was converted to its benzhydrazide (**4**) by treating with hydrazine hydrate in ethanol. The synthesis of these compounds is reported earlier.[18] The

View Article Online
DOI: 10.1039/C7NJ05136K

benzhydrazide (**4**) was further treated with 4-Cyanobenzoylchloride (**3**) in presence of triethylamine in THF. The compound obtained was subjected to $POCl_3$ mediated dehydrocyclisation to give compound **2**. These compounds were then treated with NaN_3 and NH_4Cl in DMF, to obtain the target tetrazole **1**, through Huisgen 1,3-dipolar cycloaddition reaction. The target molecule obtained was insoluble in common organic solvents and found to be soluble in highly polar solvents like dimethylformamide (DMF) and dimethylsulfoxide (DMSO), on heating. It had a good thermal stability at least up to 279 ^{o}C, as evidenced from TGA (See the Fig. S13). All the synthesized compounds were characterized by ^{1}H NMR, ^{13}C NMR, IR and Mass spectrometry. We were unable to get ^{13}C NMR of the target compound due to the gelation. The characterization data is provided in the electronic supporting information (ESI).

Gelation studies

Considering the molecular structure containing heterocyclic aromatic ring, which provide ample scope for π–π and dipole-dipole interaction, presence of three long alkyl chains that provide hydrophobic/van der Waals interaction and the presence of a tetrazole ring, which provide H-bonding interaction, we assumed that the molecule **1** would be able to self-assemble to form an organogel (Fig.1).

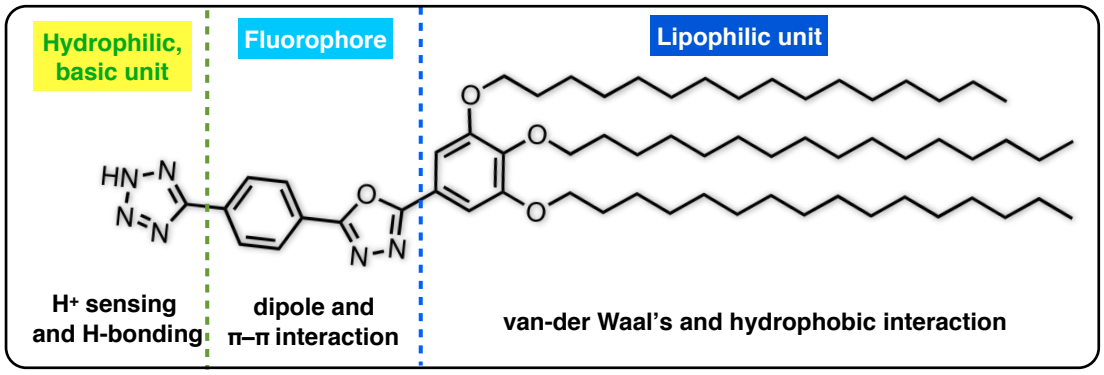

Figure 1. Molecular design of organogelator **1**

Compound **1** was insoluble in most of the common polar and apolar solvents, aromatic solvents and halogenated solvents. However, it was soluble in dimethylsulfoxide (DMSO) up on heating. Allowing the solution to stand at room temperature for 20 minutes, led to the formation of

View Article Online
DOI: 10.1039/C7NJ05136K

organogel. This is confirmed by the no flow of the material on inversion of the container (Fig.6). The critical gelation concentration (CGC) was also calculated, which was found to be 0.6 wt% in DMSO and the thermal stability (T_{gel}) of the gel was found to be 45 ^{o}C using 'dropping ball method'. This compound comes under the class of 'supergelators' because of the low CGC value.[19] Temperature dependent ^{1}H-NMR spectra of the organogel of compound **1** were recorded in DMSO-d_6 regularly at temperature intervals of every 10 ^{o}C, on heating from room temperature. A clear transformation from gel to sol was observed from the overlay of NMR spectra (Fig.2). From the figure 2, it is obvious that at lower temperature *i.e.* below T_{gel} the peaks at around 8.1 – 8.25 ppm were broad due to stronger interaction in the gel form. Upon increasing temperature, the peaks became sharper and showed the splitting due to weakening of intermolecular interactions. The gel was stable at least up to a month in closed vial at ambient temperature.

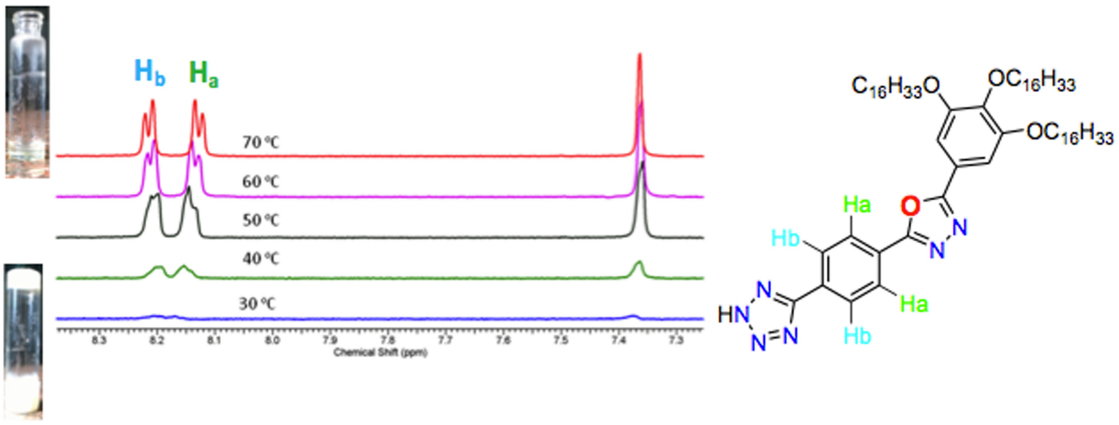

Figure 2. Expanded region of the temperature dependent ^{1}H-NMR spectra of compound **1** in DMSO-d_6.

The organogel was further characterized by photophysical studies in DMSO solution. The absorption spectrum of the solution at micromolar concentration showed a band at 318 nm, while the emission spectrum obtained by exciting at the absorption maximum showed an emission maximum at 414 nm with a Stoke's shift of 76370 cm^{-1} (Fig. S9a). The optical band gap calculated from the onset of absorption was 3.24 eV. The self-assembly could be explored by the concentration dependent UV-Vis spectroscopy, but at higher concentration the absorbance of the compound exceeded the limits of the instrument and hence we concentrated on the concentration dependent fluorescence. We measured the fluorescence spectrum as a function of temperature, from the clear solution of the compound at higher temperature to room temperature. On

decreasing the temperature, the emission spectrum showed a red shift along with a decrease in the intensity (Fig.3a-b). The shift in the emission as well as decrease in the intensity of luminescence is due to the aggregation and associated quenching. The same behavior was noticed with the lapse of time from the point of clear solution (Fig.3c-d). The solution, which exhibited a higher luminescence when just dissolved, showed a decrease in the emission intensity with a concurrent red shift with time and gets saturated at 20 min, *i.e.* on complete gelation. The gel formed was reversible for many cycles of heating and cooling, as seen by the change in the emission intensity at its emission maximum (Fig.4a). The micromolar solution of compound **1** in DMSO also showed the presence of aggregates as evidenced by the dynamic light scattering (DLS) experiments. The size of the aggregates was found to be approximately 240 nm (Fig.4b). Characterization of the morphology of the xerogel film was carried out (after the evaporation of the solvent) using Atomic Force Microscope (AFM) and field emission scanning electron microscope (FE-SEM).

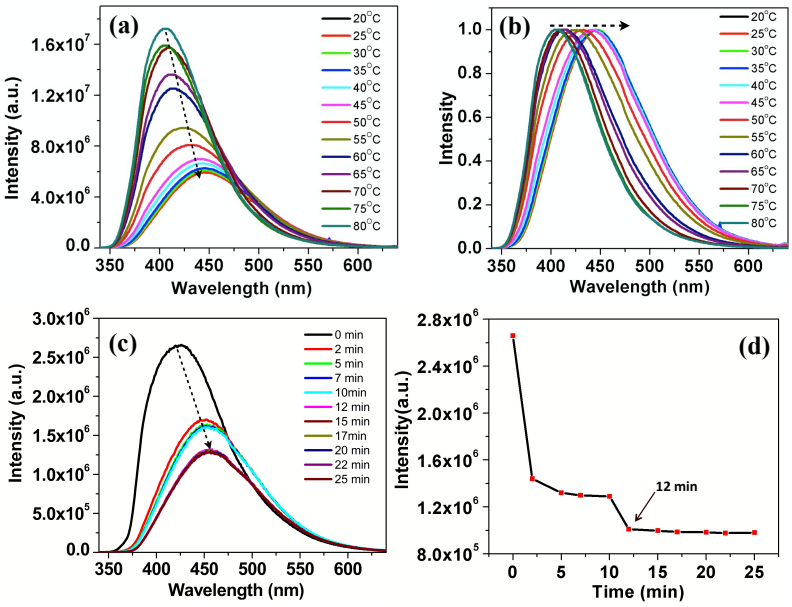

Figure 3. (a) Emission spectra as a function of temperature; (b) Normalized emission spectra with respect to temperature; (c) Emission spectra as a function of time; (d) Plot showing the change in emission intensity with respect to time at ambient temperature (concentration: 7.2 mM in DMSO, λ_{exc} = 318 nm).

View Article Online
DOI: 10.1039/C7NJ05136K

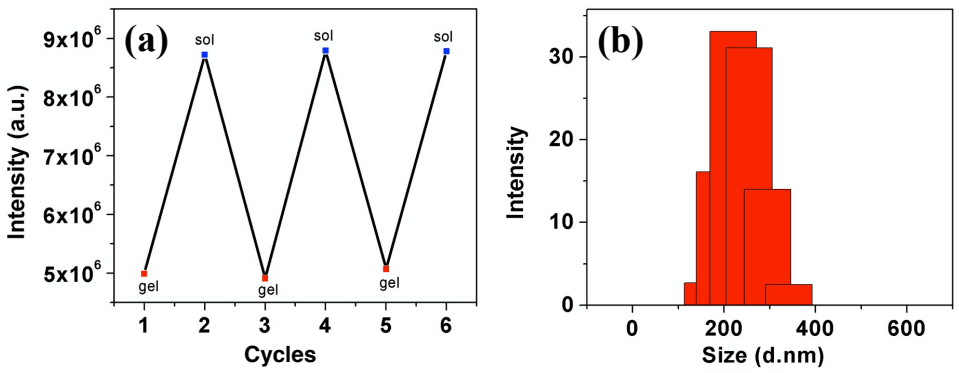

Figure 4. (a) Reversible change in the emission intensity at the emission maximum on repeated sol–gel transitions (concentration: 7.2 mM in DMSO, λ_{exc} = 318 nm); (b) DLS profiles of the 20 micromolar solution of compound **1** in DMSO.

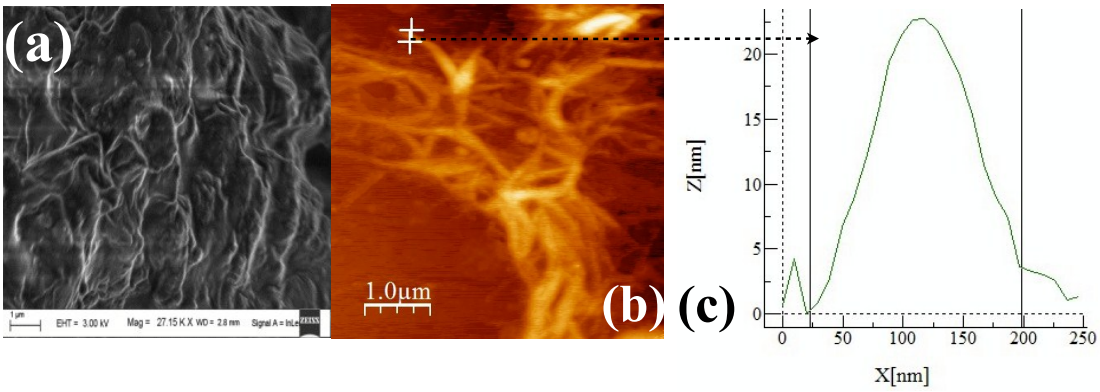

Figure 5. FE-SEM image (a); and AFM image (b) of the xerogel films of compound **1** obtained by the slow evaporation of 50 micromolar DMSO solution (scale bar: 1µm); Expanded region of a fiber in (b) showing the thickness of an individual fiber (c).

These images showed the presence of an entangled network of interwoven fibers of several micrometers in length and an average thickness of 180 nm (Figure 5).

Further, we have tested the sensing ability of the gel of compound **1** towards PA. To the gel formed with the CGC (7.2 mM in DMSO), we have added the solution **1** and PA in equimolar amounts (7.2 mM in DMSO). The gel was destabilized and converted into solution. This shows that the addition of PA destabilized the gelation. The destabilization of the gel is explained as below (Fig.6b). The organogel is formed by the intermolecular hydrogen bonding between the two tetrazole moieties of molecule **1**. This is further supported by the nanophase segregation of incompatible molecular subunits like flexible chains and hard aromatic cores. The

View Article Online
DOI: 10.1039/C7NJ05136K

self-assembly of these molecules leads to the formation of long fibers, which entrap a large volume of solvent to form a stable gel. With the addition of PA, the hydrogen bonded self-assembly of compound **1** is broken, and thus dismantling this delicate organization. This was also perceived visually under the irradiation of the UV light of longer wavelength (λ = 365 nm) with a change in the emission color (Fig.6a). This observation motivated us to study the response of compound **1** to various nitroaromatic explosives to understand the selectivity and sensitivity.

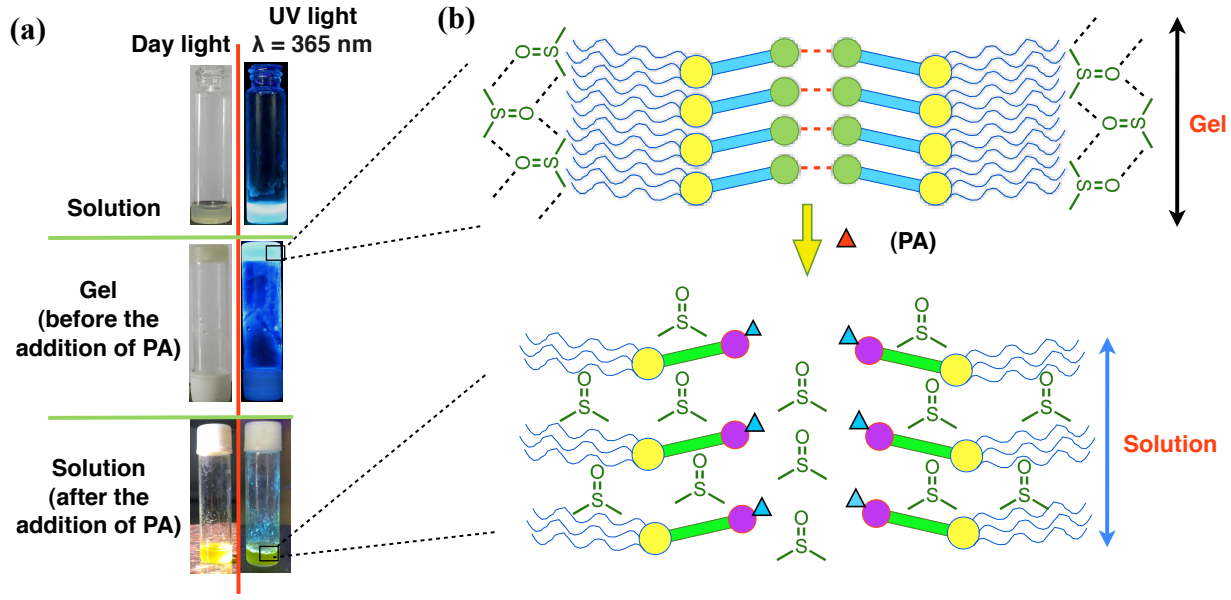

Figure 6. Photographs of the images of solution and gel under daylight and UV light of 365 nm, and response of the gel after the addition of PA (a); Schematic showing the destabilization of the gel of compound **1** in DMSO after the addition of PA (b).

Response to nitro aromatic explosives

Caution! The nitroaromatic compounds used in this study, especially TNT and PA, are very powerful explosives. They must be handled with care and also in very small quantities.

Considering the ability of the molecule to exhibit emission in solution as well as in gel state along with the presence of a basic azole moieties, we envisaged that this could be a potential molecule to sense nitrophenol based explosives. Interestingly, the compound showed a very good sensing ability towards PA in the presence of various nitro aromatic explosives (NAEs) in the solution state. The detailed results are presented as below. In order to analyze the

View Article Online
DOI: 10.1039/C7NJ05136K

sensing behavior of compound **1** toward nitro explosives in solution state and also to explore its selectivity towards PA, fluorometric titration studies were performed in presence of various common NAEs (Fig.7). An experimental solution containing compound **1** and any nitro compounds *viz.* 4-nitro toluene (4-NT), 2,4-dinitro toluene (2,4-DNT), 2,6-dinitro toluene (2,6-DNT), benzoic acid (BA), 4-nitrobenzoic acid (4-NBA), 2,4-dinitrobenzoic acid (2,4-DNBA), nitrobenzene (NB), *m*-dinitrobenzoic acid (*m*-DNB), nitromethane (NM), 4-nitrophenol (4-NP), 2,4-dinitrophenol (2,4-DNP) were taken in DMSO (1 mM solution in DMSO) (Fig.8a).

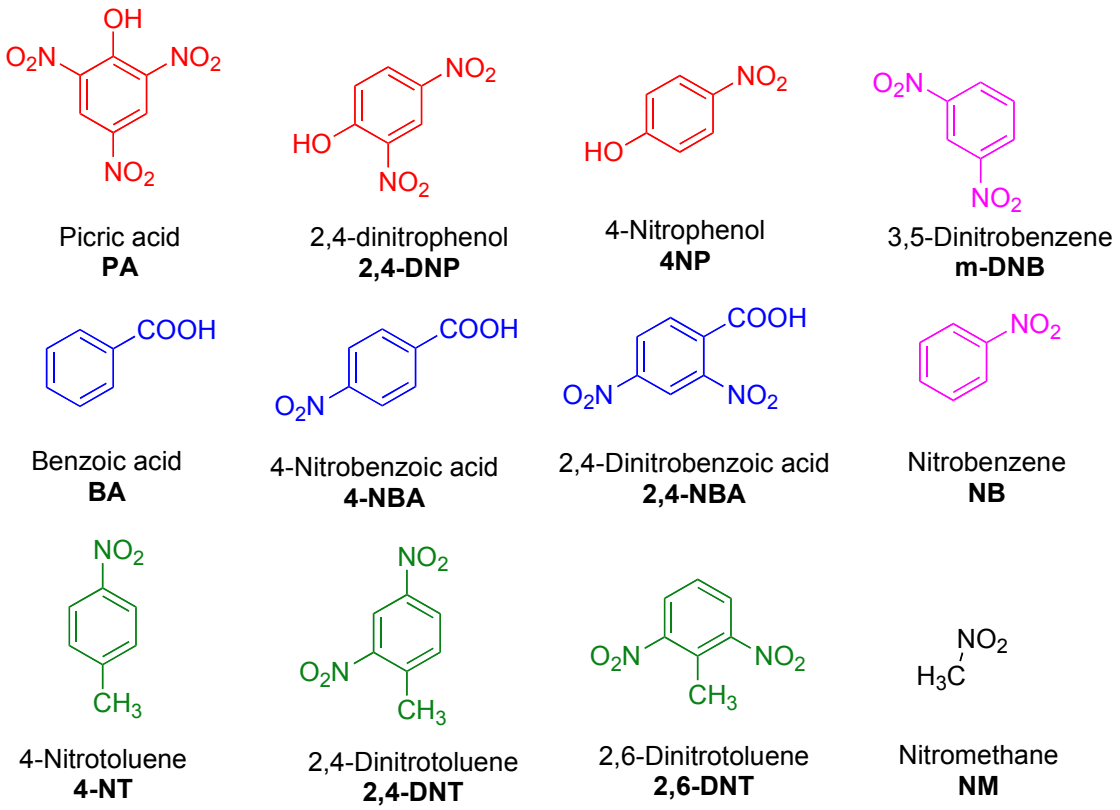

Figure 7. Structures of different nitro compounds used in this study

The emission of **1** displayed a significant change upon the addition of PA thus make it as an interesting sensor for the detection of PA (Fig. 8a-b). It has been observed that compound **1** showed this selective response even in the presence of other nitro compounds (Fig. 8c). An immediate shift in the emission maximum (449 nm) of compound **1** was observed upon adding equimolar solution of PA to compound **1** in DMSO solvent (Fig.9). The emission maximum was

414 nm for the neat solution of **1**, but shifted to 486 nm after the addition of PA (Fig. 8a,b). The red shift of 37 nm was observed in the emission spectrum after the addition of PA to the compound solution. This leads to disappearance of blue emission of compound **1** along with the appearance of green emission, which could be visualized under UV light of long wavelength (lamp excitation-365 nm) (Fig. 9). Interestingly, most of the nitro compounds used in the present study did not produce any significant changes of emission color of compound **1** (Fig.8b and 9). Though 2,4-DNP and 4-NP shift the emission of compound **1** towards green, the emission was very weak compared to that in presence of PA (Fig.8a and 9). In order to validate the selectivity of compound **1**, its fluorescence shifting by PA was performed in the presence of different nitro compounds. It is important to point out that compound **1** showed remarkable response toward PA even in the presence of various common interfering nitro group containing analytes (Fig. 8c). The selective response to PA was also seen unaltered in the presence of common anions (Fig.S11).

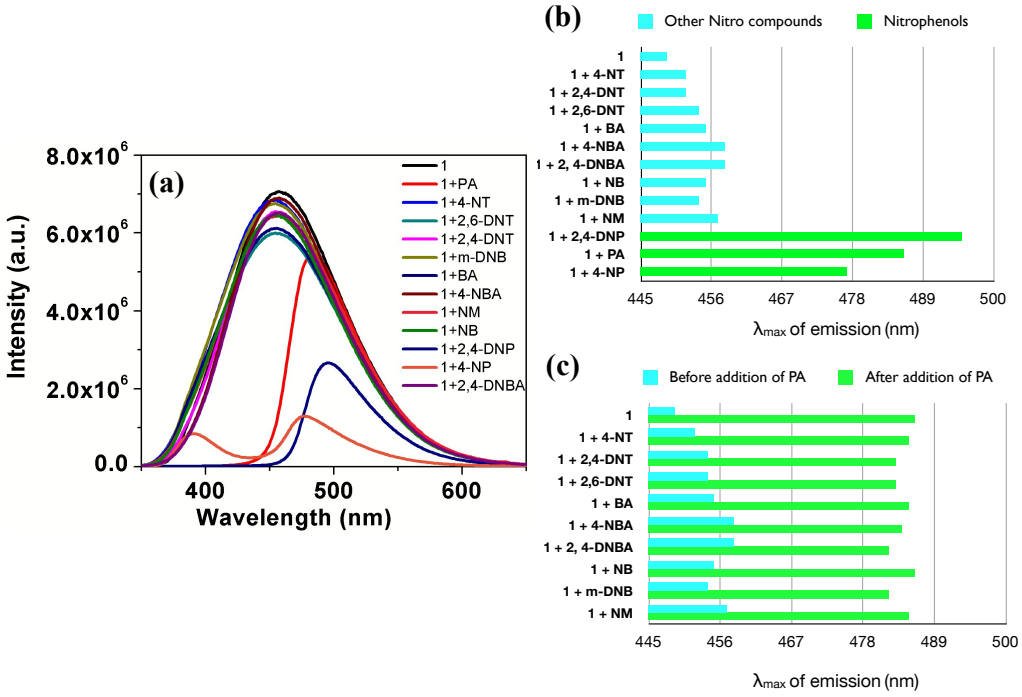

Figure 8. Emission spectra of compound **1** and its equimolar solutions with different nitro compounds (Concentration: 1 mM solution in DMSO) (a); Fluorescence response to the different nitro compounds by DMSO solution of **1** (b); Fluorescence response to the PA in presence of different nitro compounds by DMSO solution of **1** (c).

View Article Online
DOI: 10.1039/C7NJ05136K

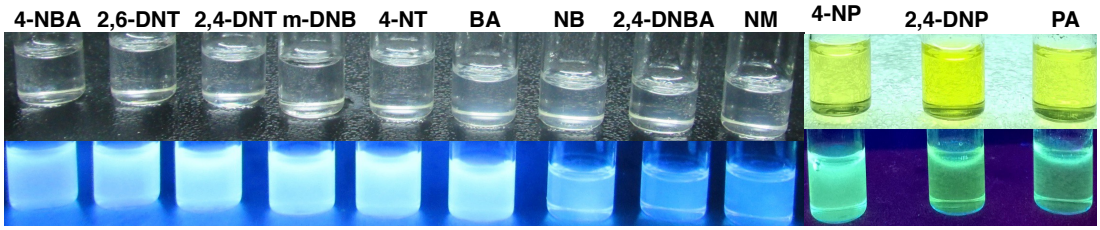

Figure 9. Images of equimolar solutions of compound **1** and nitro compounds in daylight (upper row); under UV light of long wavelength (lower row) (Concentration: 1 mM solution in DMSO).

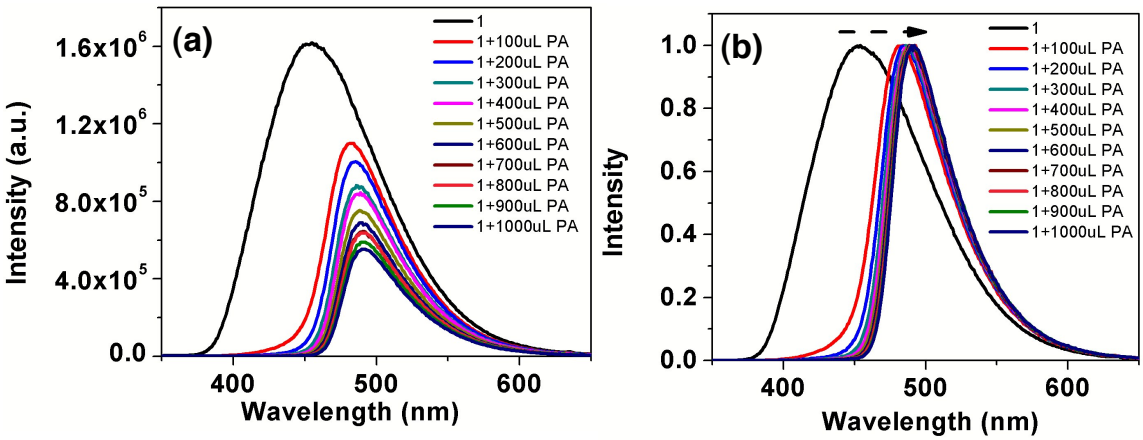

Figure 10. Emission spectra of compound **1** on the incremental addition of a mixture of PA and compound **1** (a); normalized version of the emission spectra of compound **1** obtained after the incremental addition of a mixture of PA and compound **1** (b) (Equimolar concentration; 1 mM in DMSO; Each 100 µL added had equal amount of PA and compound **1**).

In order to explain the shifting of emission from blue to green, fluorimetric titration of PA to compound **1** was carried out. This was done by an incremental addition of 0.1 mL of PA solution (100 µM) to a 1 mL solution of compound **1** in DMSO (100 µM). In order to avoid the dilution effect, we have added the same amount of compound as with the PA. It was observed that, there is a sudden shift in the emission change in the emission intensity (λ = 449 nm) of compound **1** to form a new band at around 486 nm. Further addition decreased the intensity of the band. The normalized emission spectra showed a clear red shift in the emission after the PA addition with a 37 nm red shift (Fig.10). This indicated the formation of a new species, which was further justified with the help of time resolved photoluminescence spectroscopy where the

View Article Online
DOI: 10.1039/C7NJ05136K

addition of micromolar solution of PA to a micromolar solution of **1** showed the formation of a new species with longer lifetime (Fig. 11). The fluorescence lifetime of the solution of compound **1** in DMSO at a 20 μM concentration was measured by monitoring at its emission maximum (403 nm) showed the presence of two excited species, one with a lower lifetime of [τ_1 = 1.1 ns (34%)] and other with a longer lifetime [τ_2 = 2.5 ns (66%)]. The solution of compound **1** with PA also exhibited two excited species but with longer life times [τ_1 = 2.1 ns (30%)] and [τ_2 = 8.3 ns (70%)] in comparison to compound **1** without PA.

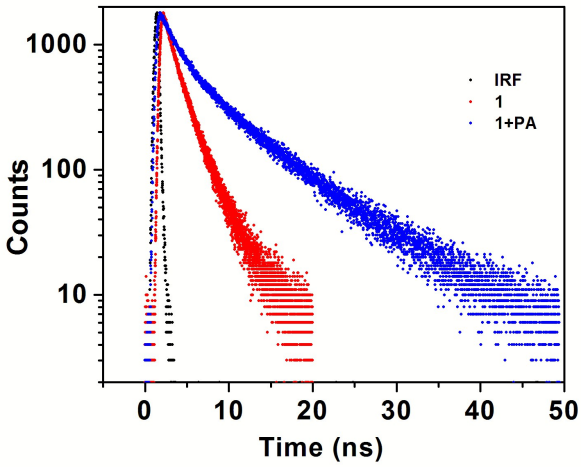

Figure 11. The fluorescence decay profiles of compound **1** in DMSO at 10 μM solution (red trace) and after the addition of PA (5 μM solution in DMSO) (blue trace) (black trace is instrument response function: IRF; λ_{exc} = 290 nm)

It is to be noted that when the titration was carried out, by using an equimolar solution of PA in water to the solution of compound in DMSO, there was a red shift in the emission band, along with a concomitant decrease in the intensity of the new band (Fig.12). This emission intensity was reduced to a minimum when the addition of PA completed one equivalent with respect to compound **1**. Thus, it is interesting to note that compound **1** could be able to detect the PA dissolved in water, which acts as a common contaminant. Though we observed a red shifted emission, the emission intensity is reduced in presence of water, which may be due to the quenching of the emission by water.

View Article Online
DOI: 10.1039/C7NJ05136K

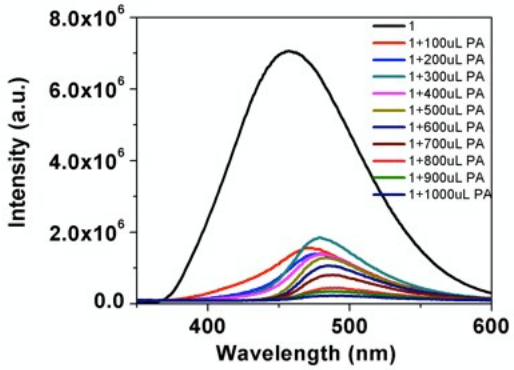

Figure 12. Emission spectra of compound **1** on the gradual addition of picric acid in water (Concentration: 1mM of compound 1 in DMSO; 1mM of PA in water, gradual addition of 0.1 mL).

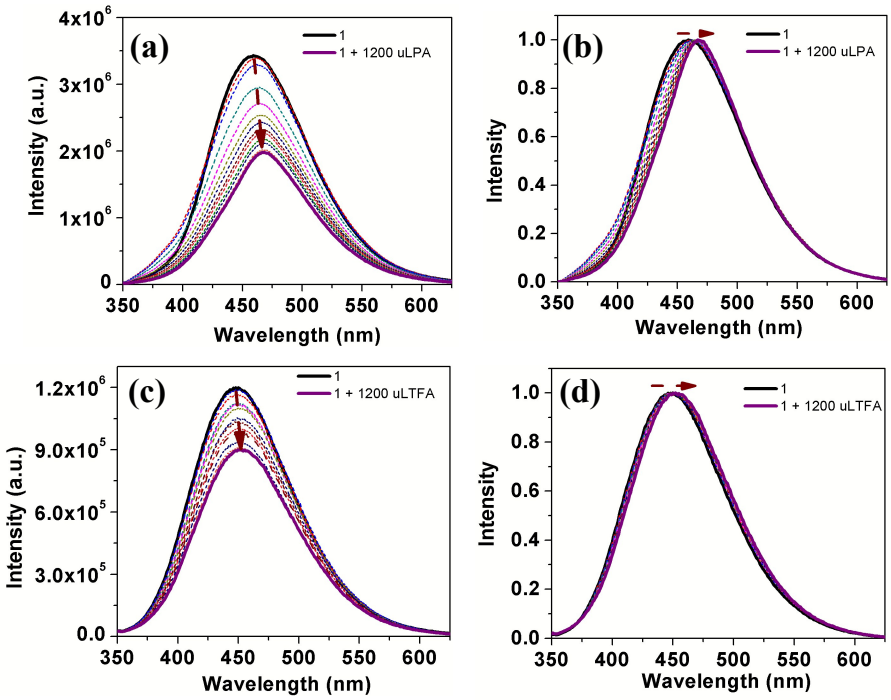

Figure 13. The fluorimetric titration of PA solution (100 μM in DMSO) to the solution of compound **1** in DMSO (10 μM in DMSO) (a); Normalized version of the same (b); The fluorimetric titration of TFA solution (100 μM in DMSO) to the solution of compound **1** in DMSO (10 μM in DMSO) (c); Normalized version of the same (d) (Each spectrum is taken after the addition of every 100 μL)

These observations pointed towards the possibility of the formation of a protonated species on the addition of PA to the solution of compound **1** in DMSO, due to the protonation of compound **1**. Considering the low pKa value of PA (0.38) and the basicity of the tetrazole ring, this is most

View Article Online
DOI: 10.1039/C7NJ05136K

probable. To test our hypothesis, we have carried out the titration of trifluoroacetic acid (TFA) in DMSO (concentration: 10 μM in DMSO) to the solution of compound **1** in DMSO (100 μM in DMSO). The gradual addition of TFA solution to the solution of compound **1** in DMSO showed a red shifted emission with a concurrent reduction in the intensity (Fig.13c,d). Similar titration was carried out with a PA solution (100 μM in DMSO) against the solution of compound **1** in DMSO (10 μM in DMSO) quenches the fluorescence of compound **1** (Fig.13a,b). Therefore, the perturbation in the emission spectrum in the presence of PA may be due to formation of protonated species. However, the redshift observed in the case of titration with PA is relatively larger than in the presence of TFA (Fig.13a,b).

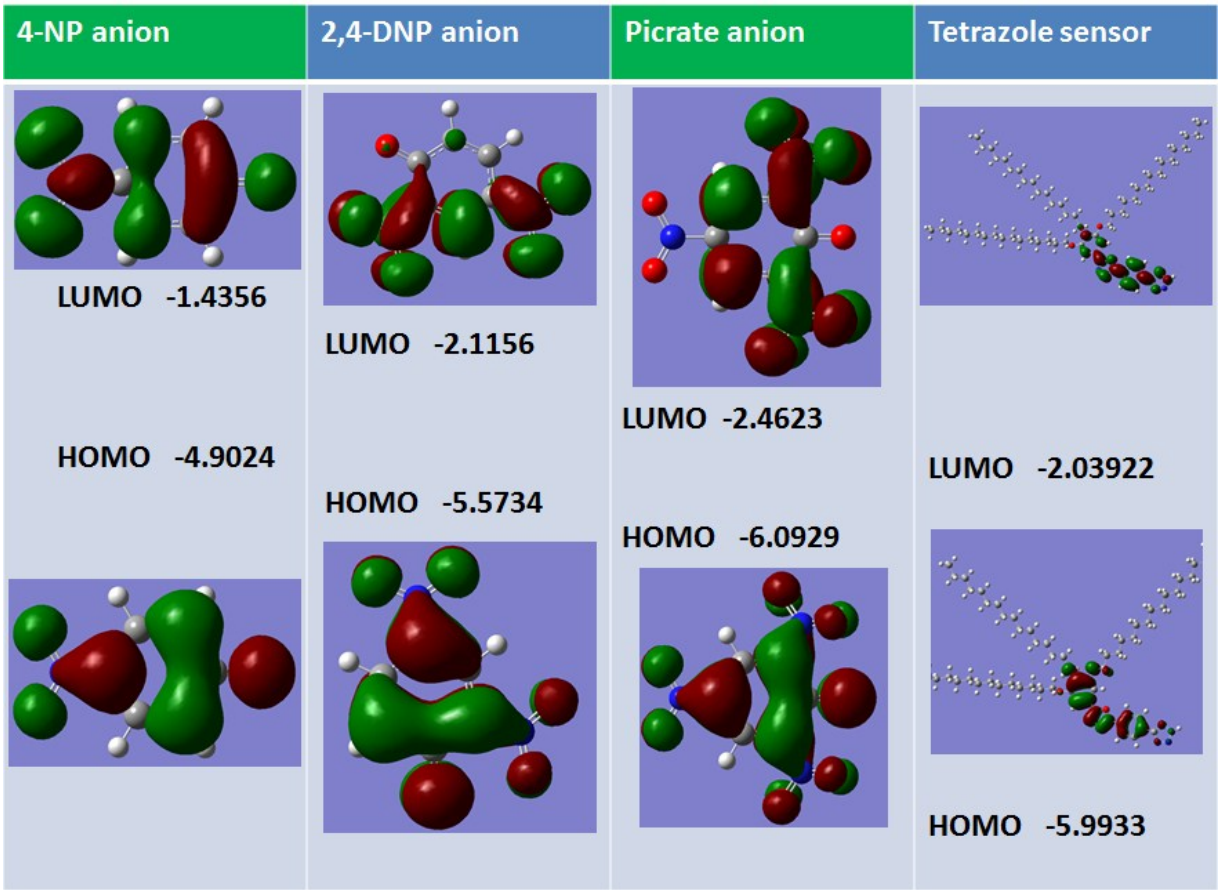

Figure 14. HOMO and LUMO orbitals of 4-nitrophenolate anion, 2,4-dinitrophenolate anion, picrate anion and compound **1**.

View Article Online
DOI: 10.1039/C7NJ05136K

Most of the fluorescent sensors developed for the detection of picrate ion were based on the quenching of fluorescence. The electron transfer from electron rich picrate anion to the sensor was reported as the mechanism of detection of picrate ion. But in the present case, upon addition of PA a red shift was observed in the emission spectrum of compound **1**. Further to rule out that the electron transfer from picrate anion to compound **1**, we have carried out the Density Functional Theory (DFT) calculations. The DFT studies shown that the energy of the highest occupied molecular orbital (HOMO) of the free compound **1** is –5.99 eV, while that of the lowest occupied molecular orbital (LUMO) is –2.04 eV. In comparison the HOMO and LUMO levels of the picrate anion are found to be –6.09 eV and –2.46 eV respectively. Thus, the energy level of the HOMO of picrate anion is lower than that of LUMO level of compound **1** (Fig.14). The actual experimental result describes that shift in emission is observed in response for the picrate anion.

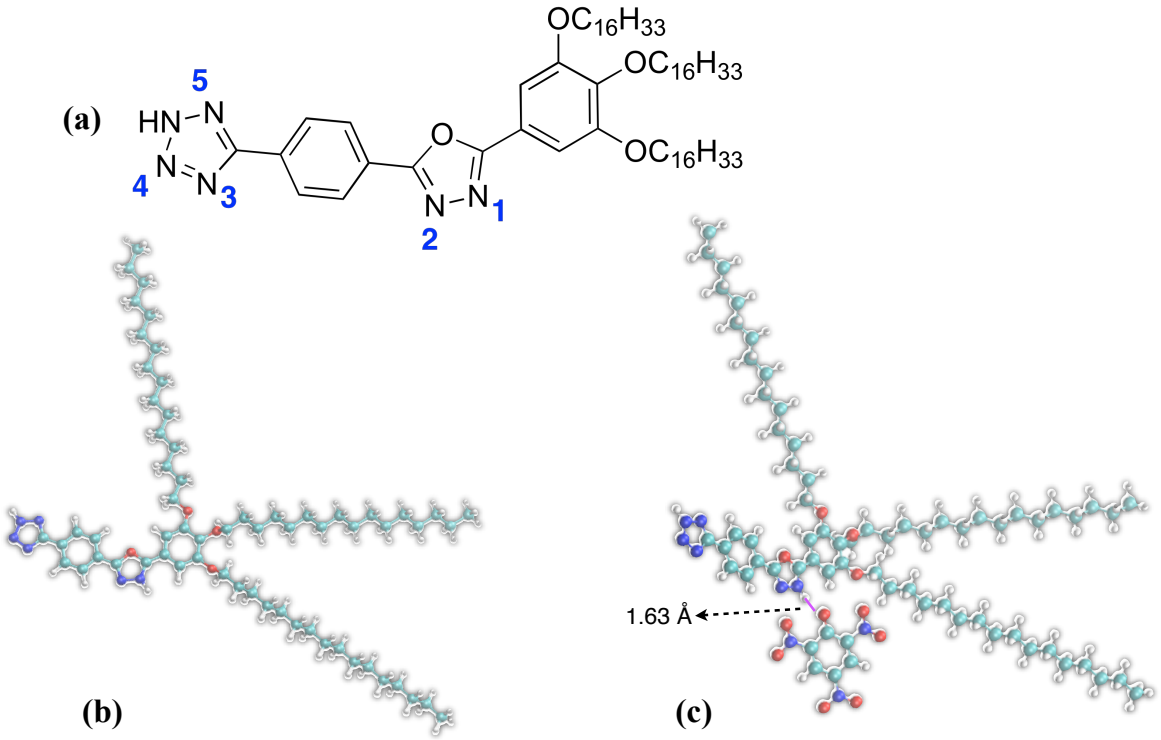

Figure 15. Structure of compound **1** showing the possible sites of protonation (a); Energy minimized structure of HA1 (b); Energy minimized structure of the complex formed between HA1 and picrate anion (c).

The other possibility is that, the new species formed by the addition of PA to the solution of compound **1** in DMSO is due to the protonation of compound **1**. Considering the low pKa value of PA (0.38) and the basicity of the azole rings, this is most probable. There are five basic centers that are available for the protonation two nitrogens on oxadiazole ring and three nitrogens on the tetrazole ring are the possible sites for protonation (Fig. 15a). The optimized structures of protonated tetrazole compound can be found in the supplementary information (Fig. S15). Among the 5 possible protonated compounds the DFT calculations suggest that HA1 is the most stable cation (Fig.15b, Table 1) in the presence of DMSO solvent. To understand further DLS and FESEM studies were carried out in the presence and the absence of PA. The DLS study showed that the average size of the particle is enhanced in presence PA compared to that in the absence of PA (Fig.17). This indicates the formation of large size particle by aggregation (Fig.16). However, just the protonation of fluorophore cannot explain the increase in size of the particle. The protonated molecule might form the hydrogen bonded complex with picrate anion and this aggregation could cause the enhancement in particle size. Such hydrogen bonded complex between the protonated sensor and picrate anion was reported.[20] The change in surface morphology in presence of PA further support this (Fig.16b). The surface morphology and DLS profiles of the protonated complex obtained from TFA addition, are different than that obtained by PA addition (Fig. 16c and 17c). To substantiate the complex formation between the HA1 and picrate anion DFT calculations were performed on HA1, picrate anion and the complex. The stabilization energy thus obtained for complex is 70.6 $kJmol^{-1}$, *i.e*. the energy of this complex is lower than the sum of the energies of HA1 and picrate anion; and HA1 alone.

Table 1. Optimized energies of the compounds considered in this study.

Compund name	Energy (kJ/mol)
Protonated tetrazole-5 (HA1)	-8124451.6
Protonated tetrazole-4 (HA2)	-8124447.5
Protonated tetrazole-3 (HA3)	-8124416.7
Protonated tetrazole-2 (HA4)	-8124366.1
Protonated tetrazole-1 (HA5)	-8124374.6
Picrate anion	-2416824.2
Protonated tetrazole (HA1)-picrate complex	-10541346.4

View Article Online
DOI: 10.1039/C7NJ05136K

The distance between hydrogen of protonated compound and oxygen of picrate anion is 1.63 Å (Fig.15c), while the distance between donor and acceptor of this hydrogen bond is 2.65 Å, suggesting a strong hydrogen bond, which could be mostly electrostatic. No imaginary frequencies were found in all these optimization calculations, suggesting that these structures are minimum points on the potential energy surface. We used B3LYP hybrid density functional and 6-31G(d) basis set for all the calculations. More importantly we performed all these calculations considering the presence of solvent (DMSO) using Polarizable Continuum Model (PCM) as implemented in Gaussian 09.

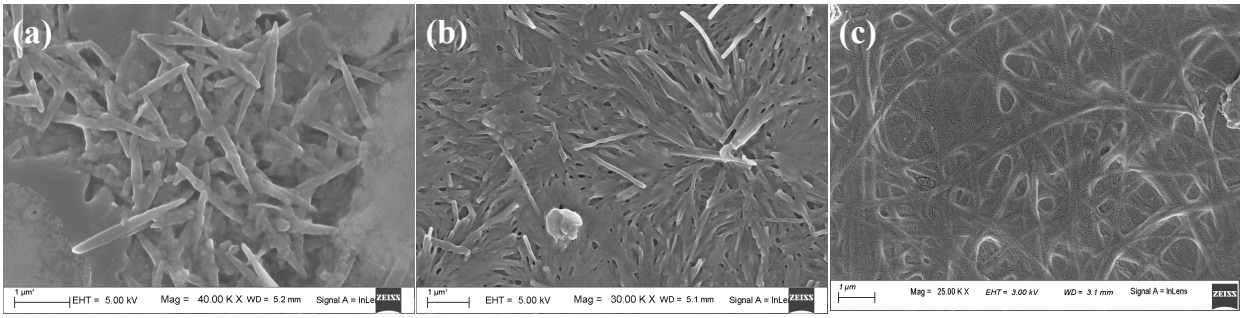

Figure 16. SEM image of the film formed by the solution of compound **1** in DMSO (1 mM in DMSO); SEM image of the film formed by the solution of compound **1** in DMSO and PA (1 mM in DMSO) (b); SEM image of the film formed by the solution of compound **1** in DMSO and TFA (1 mM in DMSO) (c).

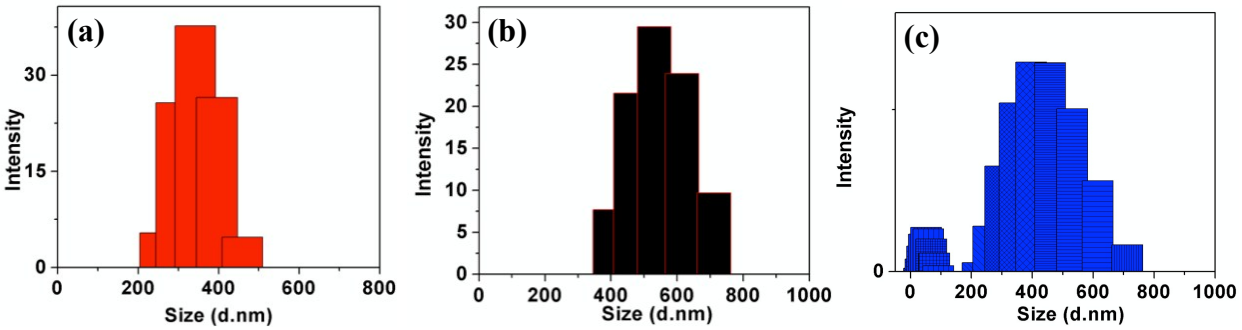

Figure 17. DLS profile of the solution of compound **1** (1 mM in DMSO) (a); DLS profile of the compound **1** and PA solution (1 mM in DMSO) (b); DLS profile of the compound **1** and TFA solution (1 mM in DMSO) (c).

Following facts further supports this hypothesis. PA is reported to deprotonate and form picrate ions in DMSO under normal condition. This is visualized by the red-shifted absorption

maximum of PA in DMSO (λ_{max} = 379 nm) in comparison to the absorption maximum in chloroform (λ_{max} = 333 nm) (See Fig. S12). The red shifted emission is observed from compound **1** only in the presence of nitrophenols, which donate acidic protons. On the other hand, only quenching is observed in other nitro compounds. This confirms that emission is due to the protonated species, which aggregates with picrate anion. The aggregation of protonated compound **1** with picrate anion is expected to reduce the solvent solute interaction, which reduces the fluorescence lifetime. Thus, the enhancement in the fluorescence lifetime of compound **1** in the presence of PA, further support this hypothesis. This means that the observed spectral changes are due to formation of new complex with picrate. The complex is formed by the interaction of protonated compound **1** with picrate ion and is not due to electron transfer. Further the selectivity of the sensor to PA is due to its lower pK_a value in comparison to 4-NP and 2,4-DNP. Among the nitrophenols, the PA has lower pK_a value. Therefore, the protonation of compound **1** and aggregation of that with counter anion are expected to be more in the presence of PA than with other two nitrophenols. Accordingly, a strong green emission is observed in the presence of PA and the emissions are weak in the presence other nitrophenols (Fig.8a,b and 9). To visualize the change in compound **1** in response to the incremental addition of PA was attempted with ^{1}H NMR, but found that the protonated species of compound **1** was not clearly soluble even at a temperature of 65 ^oC. This failed our attempt to detect the changes by NMR spectra. However, the DFT calculations clearly support the complex formation.

Further we were interested to investigate the limit of detection (LOD) of PA by compound **1**. This was carried out, considering the emission quenching response of compound **1** in response to PA at low concentration (Fig.13a,b). Six different sample solutions of compound **1** (100 μM) in DMSO were prepared. Each solution was added with different amount of PA (0 nM, 10 nM, 20 nM, 30 nM, 40 nM and 50 nM) and then the fluorescence spectrum was recorded for each sample by exciting at 318 nm. The detection limit plot for PA was obtained by plotting a change in the fluorescence intensity *vs* the concentration of PA (Fig.S14a). The plot demonstrates a linear relationship and the correlation coefficient (R^2) *via* linear regression analysis and was found to be 0.979. Stern-Volmer plot also showed the similar trend (Fig.S14b). The LOD value was then calculated[21] using the equation 3σ/K, where σ denotes the standard deviation for the intensity of compound **1** in the absence of PA and K represents slope of the equation. The value of LOD was found to be 700 ppt. As mentioned earlier, there are several

fluorescent sensors reported for the detection of PA mainly by fluorescence quenching.[22] But fluorescence quenching may be interfered by other competitive quenching processes and may not be always accurate. However, the present work is promising because of the highly selective detection of PA with a change in the fluorescence, along with a high sensitivity of parts per trillion levels. Further we are interested in developing a handheld device[23] and also to increase the sensitivity further with an improved molecular design, from the knowledge derived from the above studies.

CONCLUSION

In summary a novel organic super gelator was developed, which is only soluble in DMSO and forms a stable gel. The compound has potential application in picric acid sensing in solution state with a rarely observed shifting of emission maximum in response to the analyte. The compound in its organogel form can also be utilized for the detection of the explosive picric acid as seen by its destabilization of the gel and change in the emission. The mechanism behind this efficient detection could be the formation of complex between the protonation sensor the picrate anion. This produces a visible change emission color. Theoretical and experimental studies revealed that the sensing property is not due to ground state electron transfer. The selectivity to picric acid is due to the ease of deprotonation, which is in turn related to the pKa value of the compound. To the best of our knowledge this is the first example of tetrazole based supergelator which can detect powerful explosive picric acid with a fluorescence switching in the visible region. This compound has a high sensitivity towards the picric acid detection at parts per trillion level. This compound holds promise for the application in pollution control, border and homeland security, and humanitarian efforts during wars due to its high sensitivity, selectivity and ease of handling.

EXPERIMENTAL

Commercially available chemicals were used without any purification. Chromatography was performed using neutral alumina. For thin layer chromatography (TLC), pre-coated aluminum sheets with silica gel were employed. IR spectra were obtained on a Perkin Elmer IR spectrometer at room temperature by using KBr pellet. The spectral positions are given in wave number (cm^{-1}) unit. NMR spectra were recorded using Varian Mercury 400 MHz (at 298K) or Bruker 600 MHz NMR spectrometer. For ^{1}H NMR spectra, the chemical shifts are reported in ppm relative to TMS as an internal standard. Coupling constants are given in Hz. Mass spectra

were determined by MALDI-TOF mass spectrometer using α-cyano α-hydroxycinnamic acid as a matrix or High Resolution Mass Spectrometer. The melting point was detremined by employing a polarizing optical microscope (POM) (Nikon Eclipse LV100POL) equipped with a programmable hot stage (Mettler Toledo FP90). Clean glass slides and glass coverslips were employed for the polarizing optical microscopic observations. Thermogravimetric analysis (TGA) was performed using thermogravimetric analyzer (Mettler Toledo, model TG/SDTA 851 e) under a nitrogen flow at a heating rate of 10 °C/min. UV-Vis spectra were obtained by using Perkin-Elmer Lambda 750, UV/VIS/NIR spectrometer. Steady State anisotropy experiment and Fluorescence emission spectra in solution state and thin film state were recorded with Horiba Fluoromax-4 fluorescence spectrophotometer. Time resolved lifetime measurements were done on time correlated single photon counter from Horiba Jobin Yvon. For time resolved experiment, excitation was done by 450 nm laser diode. Atomic Force microscopy (AFM) images were obtained for the spin-coated films using Agilent 5500-STM instrument. SEM images were obtained on a JEOL 7600F FESEM instrument. We used B3LYP hybrid density functional and 6-31G(d) basis set for all the calculations. No imaginary frequencies were found in all these optimization calculations, suggesting that these structures are minmium points on the potential energy surface. We used B3LYP hybrid density functional and 6-31G(d) basis set for all the calculations. More importantly we performed all these calculations considering the presence of solvent (DMSO) using Polarizable Continuum Model (PCM) as implemented in Gaussian 09. First in order to find the possible protonation site, we performed five calculations on the tetrazole molecule by bonding Hydrogen to Nitrogen atom one at a time. Out of all these five runs, one configuration (Hydrogen bonded to the nitogen atom of oxadiazole ring) found with minimum energy is proposed as the possible site for protonation. Using this protonated tetrazole and picrate anion, we performed a calculation for the total complex.

CONFLICTS OF INTEREST

There are no conflicts of interests to declare.

ACKNOWLEDGEMENTS

ASA sincerely thanks Science and Engineering Board (SERB), DST, Govt. of India and BRNS-DAE for funding this work through project No. SB/S1/PC-37/2012 and No.2012/34/31/BRNS/1039 respectively. CIF IIT Guwahati is acknowledged for the analytical

facilities. We thank the Ministry of Human Resource Development for Centre of Excellence in FAST (F. No. 5-7/2014-TS-VII).

REFERENCES

1. G. V. Perez, A. L. Perez, *J. Chem. Educ*. 2000, **77**, 910-915.
2. M. Nipper, R. S. Carr, J. M. Biedenbach, R. L. Hooten, K. Miller, *Marine Pollution Bulletin*, 2005, **50**, 1205–1217.
3. C. Beyer, U. Bohme, C. Pietzsch, G. Roewer, *J. Organomet. Chem.* 2002, **654**, 187-201.
4. (a) J. M. Sylvia, J. A. Janni, J. D. Klein, K. M. Spencer, *Anal. Chem*. 2000, **72**, 5834-5840. (b) K. Hakansson, R. V. Coorey, R. Zubarev, V. L. Talrose, P. Hakansson, *J. Mass Spectrom*., 2000, **35**, 337-346.
5. J.R.C. Junqueira, W.R. de Araujo, M.O. Salles, T.R.L.C. Paixao, *Talanta,* 2013, **104**, 162–168.
6. (a) S. Shanmugaraju, P. S. Mukherjee, *Chem. Eur. J.* 2015, **21**, 6656-6666. (b) M. Alfonso, A. Espinosa, A. Tarraga, P. Molina, *Chemistry Open*, **2014**, *3*, 242 – 249. (c) D. S. Kim, V. M. Lynch, K. A. Nielsen, C. Johnsen, J. O. Jeppesen, J. L. Sessler, *Anal. Bioanal. Chem.* **2009**, *395*, 393-400.
7. (a) Y. Jiang, H. Zhao, N. Zhu, Y. Lin, P. Yu, L. Mao, *Angew. Chem., Int. Ed.* 2008, **47**, 8601-8604. (b) Y. Ma, H. Li, S. Peng, L. Wang, *Anal. Chem.* 2012, **84**, 8415-8421. (c) S. S. R. Dasary, A. K. Singh, D. Senapati, H. Yu, P. C. Ray, *J. Am. Chem. Soc*. 2009, **131**, 13806-13812. (d) L. Feng, H. Li, Y. Qu, C. Lu, *Chem. Commun*. 2012, **48**, 4633-4635.
8. (a) Y. Yag, H. Wang, K. Su, Y. Long, Z. Peng, N. Li, L. Feng, *J. Mater. Chem*. 2011, **21**, 11895-11900. (b) Y. Z. Liao, V. Strong, Y. Wang, X. Li, X. Wang, R. B. Kaner, *Adv. Funct. Mater.* 2012, **22**, 726-735.
9. (a) V. Bhalla, A. Gupta, M. Kumar, D. S. S. Rao, S. K. Prasad, *ACS. Appl. Mater. Interfaces.* 2013, **5**, 672-679. (b) N. Dey, S. K. Samanta, S. B. Bhattacharya, *ACS. Appl. Mater. Interfaces.* 2013, **5**, 8394-8400. (c) A. Sandeep, V. K. Praveen, K. K. Kartha, V. Karunakaran and A. Ajayaghosh, *Chem. Sci.*, 2016, **7**, 4460–4467.
10. (a) S. W. Thomas, G. D. Joly, T. M. Swager, *Chem. Rev.* 2007, **107**, 1339-1386. (b) G. He, H. Peng, T. Liu, M. Yang, Y. Zhang, Y. Fang, *J. Mater. Chem.* 2009, **19**, 7347-7353. (d) Y. J. Hu, S. Z. Tan, G. L. Shen, R. Q. Yu, *Anal. Chim. Acta* 2006, **570**, 170-175. (e) H. Nie, Y. Zhao, M. Zhang, Y. Ma, M. Baumgarten, K. Mullen, *Chem. Commun.* 2011, **47**, 1234-1236.
11. (a) H. Xu, F. Liu, Y. Cui, B. Chen, G. Qian, *Chem. Commun.* 2011, **47**, 3153-3155. (b) B. Gole, A. K. Bar, P. S. Mukherjee, *Chem. Commun.* 2011, **47**, 12137-12139. (c) D. Samanta, P. S. Mukherjee, *Dalton. Trans.* 2013, **42**, 16784-16795. (d) V. Vajpayee, H. Kim, A. Mishra, P. S. Mukherjee, P. J. Stang, M. Lee, H. K. Kim, K. W. Chi, *Dalton Trans.* 2011, **40**, 3112-3115. (e) S. Ghosh, P. S. Mukherjee, *Organometallics*, 2008, **27**, 316-319. (f) S. Shanmugaraju, H. Jadav, P. Y. Patil, P. S. Mukherjee, *Inorg. Chem*. 2012, **51**, 13072-13074. (g) S. Shanmugaraju, S. A. Joshi, P. S. Mukherjee, *Inorg. Chem.* 2011,

50, 11736-11745. (h) S. S. Nagarkar, B. Joarder, A. K. Chaudhari, S. Mukherjee, S. K. Ghosh, *Angew. Chem., Int. Ed.* 2013, **52**, 2881-2885.

12. R. Ni, R. B. Tong, C. C. Guo, G. L. Shen, R. Q. Yu, *Talanta*, 2004, **63**, 251-257.
13. (a) T. M. Swager, J. H. Wosnick, *MRS Bull*., 2002, **27**, 446– 450; (b) K. Sakakibara, J. P. Hill and K. Ariga, *Small*, 2011, **7**, 1288–1308; (c) A. Rose, Z. Zhu, C. F. Madigan, T. M. Swager and V. Bulović, *Nature*, 2005, **434**, 876–879; (d) V. Bhalla, A. Gupta, M. Kumar, *Org. Lett*. 2012, **14**, 3112-3115. (e) B. Roy, A. K. Bar, B. Gole, P. S. Mukherjee, *J. Org. Chem.* 2013, **78**, 1306-1310, (f) A. Chowdhury, P. S. Mukherjee, *J. Org. Chem.* 2015, **80**, 4064-4075, (g) K. K. Kartha, A. Sandeep, V. K. Praveen and A. Ajayaghosh, *Chem. Rec.,* 2015, **15**, 252–265.
14. (a) D. Xuewen, J. Zhou, J. Shi, B. Xu, *Chem. Rev*. 2015, **115**, 13165−13307. (b) S. S. Babu, V. K. Praveen, A. Ajayaghosh, *Chem Rev*, 2014, **114(4)**, 1973-2129.
15. J-Y. Li, X.-Q. Zhou, Y. Zhou, Y. Fang, C. Yao, *Spectrochimica Acta Part A: Molecular and Biomolecular Spectroscopy*, 2013, **102**, 66–70.
16. (a) L. daSilva, H. Gallardo, R. F. Magnago, I. M. Begnini, *Mol. Cryst. Liq. Cryst.,* 2005, **432**, 1–13, (b) D. R. dos Santos, A. Gabriela, S. de Oliveira, R. L. Coelho, I. M. Begnini, R. F. Magnago, and L. da Silva, *Arkivoc*, 2008, **xvii**, 157-166. (c) M. Tariq, S. Hameed, I. H. Bechtold, A. J. Bortoluzzid and A. A. Merlo, *J. Mater. Chem. C,* 2013, **1**, 5583-5593. (d) E. Meyer, C. Zucco, H. Gallardo, *J. Mater. Chem.,* 1998, **8(6)**, 1351–1354.
17. (a) P. C. Andrews, P. C. Junk, M. Massi, M. Silberstein, *Chem. Commun.* 2006, 3317−3319. (b) M. He, J. Li, S. Tan, R. Wang, Y. Zhang, *J. Am. Chem. Soc.*, 2013, **135**, 18718−18721. (c) H. Lee, S. H. Jung, W. S. Han, J. H. Moon, S. Kang, J. Y. Lee, J. H. Jung, S. Shinkai, *Chem. Eur. J.*, 2011, **17**, 2823 – 2827 (d) S. V. Voitekhovich, A. Wolf, C. Guhrenz, A. S. Lyakhov, L. S. Ivashkevich, M. Adam, N. Gaponik, S. Kaskel, A. Eychmüller, *Chem. Eur. J.*, 2016, **22**, 14746 – 14752. (e) Y. Hu, M. Ding, X.-Q. Liu, L.-B. Sun and H.-L. Jiang, *Chem. Commun*., 2016, 52, 5734-5737. (f) V. Bhalla, A. Gupta, M. Kumar, D. S. S. Rao, S. Krishna Parasad, *ACS Appl. Mater. Interfaces*, 2013, 5, 672-679.
18. B. Pradhan, S. K. Pathak, R. K. Gupta, M. Gupta, S. K. Pal and A. S. Achalkumar, *J. Mater. Chem. C*, 2016, **4**, 6117-6130.
19. Z.-X. Liu, Y. Feng, Z.-C. Yan, Y.-M. He, C.-Y. Liu and Q.-H. Fan, *Chem. Mater.,* 2012, **24**, 3751–3757. (a) A. Gopal, R. Varghese and A. Ajayaghosh, *Chem. – Asian J.*, 2012, **7**, 2061–2067; (b) Q. Wang, J. L. Mynar, M. Yoshida, E. Lee, M. Lee, K. Okuro, K. Kinbara and T. Aida, *Nature*, 2010, **463**, 339–343; (d) H. Wang, C. Yang, M. Tan, L. Wang, D. Kong and Z. Yang, *Soft Matter*, 2011, **7**, 3897.
20. Y.-C. Wu, S.-H. Luo, L. Cao, K. Jiang, L.-Y. Wang, J.-C. Xie, Z.-Y. Wang, *Analytica Chimica Acta*, **2017**, 976, 74-83.
21. (a) M. Kumar, S. I. Reja, V. Bhalla, *Org. Lett*. 2012, **14**, 6084- 6087. (b) X. H. Zhou, L. Li, H. H. Li, A. Li, T. Yang, W. Huang, *Dalton. Trans*. 2013, **42**, 12403-12409.

22. N. Venkatramaiah, S. Kumar and S. Patil, *Chem. Commun.*, 2012, **48**, 5007–5009; (b) D. Dinda, A. Gupta, B. K. Shaw, S. Sadhu and S. K. Saha, *ACS Appl. Mater. Interfaces* 2014, **6**, 10722−10728; (c) A. Ding, L. Yang, Y. Zhang, G. Zhang, L. Kong, X. Zhang, Y. Tian, X. Tao, and J. Yang, *Chem. Eur. J*. 2014, **20**, 12215 – 12222; (d) K. Acharyya and P. S. Mukherjee, *Chem. Commun*., 2014, **50**, 15788-15791; (e) J. Ma, T. Lin, X. Pan and W. Wang, *Chem. Mater*. 2014, **26**, 4221−4229.
23. A. Hakonen, F. C. Wang, P. O. Andersson, H. Wingfors, T.Rindzevicius, M. S. Schmidt, V. R. Soma, S. Xu, Y. Q. Li, A. Boisen, and H. A. Wu, *ACS Sens.* 2017, **2**, 198−202.